

Competition Subject 1 : Optimized Design

Yoshikazu Makino*, Shinkyu Jeong*, Ken'ichiro Suzuki*
Yoshine Ueda*, Kisa Matsushima**, Kenji Yoshida*

* National Aerospace Laboratory

7-44-1 Jindaiji-higashi, Chofu, Tokyo 182-8522, Japan

** Tohoku University

01 Aoba-yama, Sendai 980-8579, Japan

Abstract

The aerodynamic design of an SST configuration with some geometry requests at given flight condition in 3rd NAL-SST-CFD workshop competition subject 1 is conducted by following three design tools: a conventional linear theory design tool, a CFD-based optimization tool and a CFD-based inverse design tool. In order to increase a lift to drag ratio(L/D) of the airplane, several design concepts are adopted such as a warp wing design, linear and non-linear area-ruled fuselage designs and a supersonic NLF (Natural Laminar Flow) wing design. The non-linear area-ruled fuselage design shows that the CFD-based optimization design tool can improve the aerodynamic properties of the airplane designed by the conventional linear theory design tool. As for the NLF wing design, however, the CFD-based inverse design tool should be carefully coordinated in order to realize the target NLF pressure distributions.

Introduction

National Aerospace Laboratory (NAL) of Japan started a scaled supersonic experimental airplane program which we call NEXST (National Experimental Supersonic Transport)[1] in 1996 in order to establish advanced technologies including a sophisticated CFD-based total design tool for the next generation supersonic civil transport. In this program, at first we will conduct flight tests of an un-manned non-powered experimental

airplane (NEXST-1) in 2002. Its design concepts for a high L/D are a cranked arrow wing, a modulated warp, an area-ruled configuration and an NLF wing. The NLF wing is designed by a NAL's original CFD-based inverse design technology[2]. In order to develop a CFD-based optimization design tool[3] for a complete airplane configuration, a jet-powered experimental airplane (NEXST-2) will be designed as a successor of NEXST-1. We utilize these CFD-based total aerodynamic design tools in the competition subject 1 in this workshop.

Design Process

The design process is shown in Table 1. At first, the 0th configuration is defined by nose and tail cones and a straight fuselage with a flat wing which means a warp design has not been incorporated yet. Next, warp design is applied to the wing by Carlson method and the aircraft configuration is defined as the 1st configuration. The 2nd configuration is defined by replacing the fuselage of the 1st configuration with an axisymmetrical area-ruled fuselage. The fuselage geometry of the 2nd configuration is modified in the design of the 3rd configuration by the CFD-based optimization tool developed in NAL's NEXST project. Finally the 4th configuration is designed by incorporating the NLF concept into the wing of the 3rd configuration by the CFD-based inverse design tool which is also developed in the NEXST project.

0th Configuration

In the design of the 0th configuration, wing planform of NEXST-1 is adopted. This wing planform is determined to minimize the drag due to lift by parametric studies shown in Figure 1. Its airfoils are defined by NACA 64A series at every span location shown in Figure 2 (a). Fuselage geometry is defined by a simple cylindrical body with nose and tail cones shown in Figure 2 (b). Top and side view of the 0th configuration is shown in Figure 2 (c).

1st Configuration

In the design of the 1st configuration, the warp design which means to adopt a combination of camber and twist distribution determined by an optimum load distribution is conducted to the wing geometry of the 0th configuration in order to reduce lift-dependent drag. Carlson method[4][5] is used in this warp design. Figure 3 (a) shows the airfoil geometries of the warped wing and Figure 3 (b) shows the twist angle distribution. Each airfoil show a leading edge droop and the airfoils are twisted down toward the wing tip.

2nd Configuration

The 2nd configuration is defined by replacing the fuselage of the 1st configuration with an area-ruled one in order to reduce supersonic wave drag due to volume. The area-ruled fuselage is defined so that the equivalent area distribution of the configuration is equal to that of the Sears-Haack body. An equivalent area distribution of a configuration is determined as follows:

- 1) Define a cutting plane at a given point on an airplane axis whose normal vector is inclined at the angle of $(\pi/2-\mu)$ to the axis. (μ : Mach angle)
- 2) Generate a cross section of airplane intercepted by the cutting plane.
- 3) Define an equivalent area as a frontal projection area of the cross sections.
- 4) Rotate the cutting plane at the angle of $2\pi/N$ around the airplane axis and calculate the equivalent area in the same way as 2) and 3).
- 5) Repeat 4) N times and average all N equivalent areas.
- 6) Repeat 1)~5) from the nose to the tail of the airplane.

Figure 4 shows the area-ruled fuselage geometry of the 2nd configuration. It shows the fuselage is constricted in the middle part due to the wing volume.

In order to evaluate and compare the aerodynamic properties for these three configurations, Euler CFD analysis code[6] using unstructured computational grid is utilized. Finite volume method is used in this CFD code and the surface grid is generated by an advancing front method. Sample computational grid and surface pressure contours are shown in Figure 5. Figure 6 (a) and (b) show the C_L - α curves and the polar(C_{Dp} - C_L) curves for these three configurations, respectively. Some aerodynamic coefficients and parameters, such as $C_{L\alpha}$ (slope of C_L - α curve), C_{Dp_min} (minimum pressure drag coefficient), L/D_{max} and so on, for the configurations are listed in Table 2. In this table, parameter K which characterize a polar curve is defined as follows:

$$C_{Dp} = K (C_L - C_{L@C_{Dp_min}}) + C_{Dp_min}$$

In Figure 6 (a), the C_L - α curve of the 0th configuration starts from the origin($C_L=0.0$ at $\alpha=0.0$ degree) for its flat(non-warped) wing and the curve shifts about 0.02 upward after the warp design of the wing. The C_L - α curve of the 2nd configuration is about the same as that of the 1st configuration. It suggests that an area-rule design doesn't change C_L - α characteristics of an airplane. Slopes of C_L - α curve($C_{L\alpha}$) for these three configurations shown in Table 2 are about the same value. $C_{L\alpha}$ seems to be mainly determined by a planform of the wing. A supersonic lifting surface theory shows that $C_{L\alpha}$ for an warped wing equals to that for a flat plate wing. As for the drag characteristics, the parameters K for these three configurations are about the same. This is natural because parameter K equals to an inverse of $C_{L\alpha}$ in supersonic lifting surface theory. Comparison between the 0th and 1st configurations, the polar curve shifts right(increase $C_L@C_{Dp_min}$ about 0.01 from 0.0 for the 0th configuration) by the warp design. Although C_{Dp_min} itself increases by the warp design, $C_{Dp}@C_{L_des}$ (C_{L_des} : design lift coefficient) decreases about 3.5 drag counts(1 drag count = 0.0001) and L/D_{max} also increases. These are effects of the warp design. $C_L@L/D_{max}$ of the warped wing is about 0.083 which is greater and nearer to the design C_L of 0.1 than that of the flat wing. C_{Dp_min} for the 2nd configuration decreases to the same level as that for the 0th configuration while its $C_L@C_{Dp_min}$ doesn't change from that for the 1st configuration by the area-rule design. $C_{Dp}@C_{L_des}$ also decreases about 5 counts from the 1st configuration. These results mean that an area-rule design can

enhances the effects of a warp design. L/D_{\max} also increases by the area-rule. $C_L@L/D_{\max}$ of the area-ruled configuration, however, becomes smaller and farther from the design C_L than that of the warped configuration.

3rd Configuration

The developed CFD-based optimization tool utilizes the ADS(Automated Design Synthesis) program[7] as an optimizer. Sensitivity analysis needed in the optimization process is conducted using the adjoint method[8] to reduce computational costs. The area-ruled fuselage geometry of the 2nd configuration is modified by this optimization tool in order to reduce supersonic wave drag due to volume. 11th order Bezier curve is used to define a radial change distribution of a fuselage cross section along an airplane axis and the geometry is modified axisymmetrically by adding this Bezier curve to the radius distribution of the initial fuselage geometry. The radial coordinates of control points for Bezier curve are used as design variables. The number of design variables is 10 in this design case. Object function to be minimized in the optimization process is pressure drag of the configuration estimated by Euler CFD analysis. Following two design constraints are imposed:

$$\text{Vol} > \text{Vol}_0$$

$$C_L > C_{L_{\text{des}}}$$

where Vol and Vol₀ represent a designed and an initial fuselage volume, respectively. Figure 7 shows the optimized fuselage geometry compared with the initial geometry of the 2nd configuration. The fore part of the fuselage becomes slender and the aft part becomes wider. Figure 8 (a) and (b) show the C_L - α curve and the polar curve for the 3rd configuration compared with the 2nd configuration. The C_L - α curve of the 3rd configuration is about the same as that of the 2nd configuration. The polar curve shifts downward and $C_{Dp}@C_{L_{\text{des}}}$ decreases about 1.5 counts by the optimization. The parameter K slightly reduces from the 2nd configuration while $C_{L\alpha}$ doesn't change. L/D_{\max} increases by the optimization.

4th Configuration

Friction drag reduction due to NLF wing design concept is one of the most effective ways to improve L/D at supersonic speed.

NAL has already developed a CFD-based NLF wing design methodology in the NEXST-1 design. This methodology is derived from a stability analysis of three-dimensional boundary layer and from an effective CFD-based inverse design method. Figure 9 shows our target Cp distribution for the inverse design of NLF wing. The remarkable feature is rapid accelerated region near the leading edge and almost flat pressure level after the acceleration. This type of Cp distribution like a step function is effective to suppress the cross-flow instability, which is dominant in transition on highly swept wings. Figure 9 also shows the NEXST-1 airfoil sections designed by the CFD-based inverse design method. Figure 10 shows transition characteristics of the NEXST-1 wing at flight condition predicted by using NAL's original e^N code. In general, transition location is predicted by assuming a transition N value corresponding to natural transition. If N=14 is selected according to NASA's results of low disturbance supersonic tunnel tests, large laminar region from the leading edge to about 40% chordwise location would be expected at the design point. However, the NEXST-1 is a scaled experimental airplane whose length is 11.5m. Therefore its flight Reynolds number is lower than that of a real SST. If the present target Cp distribution is applied to a large aircraft, large laminar region is never expected as shown in Figure 11. In order to establish our NLF wing design concept in applying to a real SST design, our target Cp distribution must be improved. At first, a new target Cp distribution is expressed using some parameters as indicated in Figure 12. Next, an optimum combination of those parameters is obtained through transition analysis for several target Cp distributions. One of the results is shown in Figure 13. The rapid acceleration becomes steeper than that of the target Cp for the NEXST-1. The new target Cp distribution is shown in Figure 14 and transition characteristics are summarized in Figure 15. Relatively large laminar region is expected even though Re number is much higher than that of the NEXST-1. Therefore, this new target Cp distribution is suitable for the design of this competition.

The developed CFD-based inverse design method is based on Takanashi's concept that uses integral equations and residual correction technique[9]. The procedure of the inverse method is shown in Figure 16.

- 1) Arbitrary initial wing geometry and the target pressure distribution are input.
- 2) Flow analysis around the input wing geometry is performed and the difference between the obtained and target pressure distribution is calculated.
- 3) With this difference, the geometry correction value is determined by solving integral equations.
- 4) The new wing geometry is determined by adding geometry correction values to initial wing geometry.
- 5) Repeat 2) ~ 4) until the difference between the target and calculated pressure distribution become small enough.

The original Takanashi's method is for subsonic and transonic wing design. It is extended to supersonic region by the following derivations:

The thickness correction related equation:

$$\Delta u_s(x, y) = -\Delta w_s(x, y) + \frac{1}{\pi} \iint_{\xi_1} \frac{(x-\xi)\Delta w_s(\xi, \eta)}{\sqrt{(x-\xi)^2 - (y-\eta)^2}} d\xi d\eta$$

$$\Delta u_s(x, y) = \Delta \phi_x(x, y, +0) + \Delta \phi_x(x, y, -0)$$

$$\Delta w_s(x, y) = \Delta \phi_z(x, y, +0) - \Delta \phi_z(x, y, -0)$$

The camber correction related equation:

$$\Delta w_a(x, y) = -\Delta u_a(x, y) + \frac{1}{\pi} \iint_{\xi_1} \frac{(x-\xi)\Delta u_a(\xi, \eta)}{(y-\eta)^2 \sqrt{(x-\xi)^2 - (y-\eta)^2}} d\xi d\eta$$

$$\Delta u_a(x, y) = \Delta \phi_x(x, y, +0) - \Delta \phi_x(x, y, -0)$$

$$\Delta w_a(x, y) = \Delta \phi_z(x, y, +0) + \Delta \phi_z(x, y, -0)$$

where Δ represents the difference between target and designed. $\Delta \phi_x$ and $\Delta \phi_z$ can be represented as follows;

$$\Delta C_{p_{\pm}}(x, \frac{y}{\beta}) = -2\beta^2 \Delta \phi_x(x, y, \pm 0), \quad \frac{\partial \Delta f_{\pm}(x, y)}{\partial x} = \beta^3 \Delta \phi_z(x, y, \pm 0)$$

where the subscript '±' denotes the upper and lower surfaces of the wing and $\beta^2 = M^2 - 1$. In this design case there are two design constraints. One is to keep the z position of 70% camber line at every spanwise section so that the axis of trailing edge flap can be penetrated and the other is to keep minimum wing thickness. In order to retain the 70% camber lines position, the camber correction value at 70% chord is set to zero at every spanwise section by shifting the correction values along z coordinate direction. The minimum wing thickness is conserved by changing the level of target pressure distribution so as to set the thickness correction at maximum thickness point to be zero. However, this procedure cannot guarantee that the generated airfoil has closure trailing edge. To eliminate this problem and keep the minimum thickness of the wing, the closure condition is applied after

the 70% chord. Closure condition is performed by the following equation:

$$\Delta w_s^{\text{mod}}(x, y) = \Delta w_s(x, y) - \frac{\int_{70\% \text{ chord}}^{\text{r.E.}} \Delta w_s(\xi, y) d\xi}{\ell}$$

where ℓ is a length from the 70% chord to the trailing edge.

In this study, inverse design was started with the 3rd configuration as an initial wing geometry. Figure 17 shows the pressure distributions of initial, target and designed wings after 6 inverse iterations. It seems that the pressure distribution of designed wing become very close to that of the target. However, our transition analysis code predicted that the transition happens from the leading edge at all spanwise section shown in Figure 18. Figure 19 shows the close-up view of pressure distributions at leading edge. The accordance with the target pressure distribution is not enough to delay transition. The shape of pressure distribution at leading edge is very important for the transition delay. Furthermore this design case is for real scale of aircraft, the Reynolds number is very high. Thus small discrepancy of pressure distribution at leading edge could be the trigger of transition. To get the high accordance, the inverse design iteration is continued. Figure 20 and 21 show the pressure distributions of initial, target and designed wings after 10 inverse iterations. With this pressure distribution, the transition analysis was performed. The result is shown in Figure 22. On the region of middle span, the transition is started to delay. However, on the region of inboard, transition still happened from the leading edge. The designated target pressure distribution is very hard to be realized. To achieve such a target pressure distribution, resolution for inverse method, especially at the region of leading edge should be carefully investigated. Figure 23 shows the spanwise load distributions for each configuration. The load distribution of the 4th configuration agree well with the target. It indicates that the inverse design can realize a preferable spanwise load distribution. Figure 24 (a) and (b) show the C_L - α curve and the polar curve for the 4th configuration compared with the other configurations. The C_L - α curve of the 4th configuration shifts upward comparing the 3rd configuration. The polar curve also shifts upward and $C_{Dp}@C_{L_{\text{des}}}$ becomes 2.8 counts larger than that of the 3rd configuration and even 1.4 counts larger than that of the 2nd configuration. This

pressure drag penalty should be compared with the reduction of friction drag due to NLF wing design. In this case, however, the reduction of friction drag seems to be very small because of the pressure discrepancy shown in Figure 21.

Concluding Remarks

The aerodynamic design of an SST configuration for the competition subject 1 is conducted by defining the 0th, 1st, 2nd, 3rd, 4th configurations which are designed using a conventional linear theory design tool, a CFD-based optimization tool and a CFD-based inverse design tool. In each design stage, the L/D of the configuration evaluated by an Euler CFD analysis is improved by adopting a warp design in the 1st configuration, an area-rule design in the 2nd configuration, a fuselage shape optimization in the 3rd configuration. An NLF wing design in the 4th configuration, however, doesn't improve the L/D. The CFD-based inverse design tool should be carefully coordinated in order to realize the target NLF pressure distributions and the reduction of the friction drag should be evaluated and compared with the pressure drag penalty.

References

1. Sakata, K., "Supersonic Experimental Airplane Program in NAL (NEXST) and its CFD-Design Research Demand," 2nd International Workshop on CFD for SST, pp53-56, 2000.
2. Matsushima, K., Iwamiya, T. and Zhang, W., "Inverse Wing Design for the Scaled Supersonic Experimental Airplane with Ensuring Design Constraints," 2nd International Workshop on CFD for SST, pp91-96, 2000.
3. Makino, Y., Iwamiya, T. and Lei, Z., "Fuselage Shape Optimization of a Wing-body Configuration with Nacelles," AIAA 2001-2447, 2001.
4. Carlson, H.W. and Middleton, W.D., "A Numerical Method for the Design of Camber Surface of Supersonic Wings with Arbitrary Planform," NASA TN D-2341, 1964.
5. Carlson, H.W. and Millar, D.S., "Numerical Method for the Design and Analysis of Wings at Supersonic Speeds," NASA TN D-7713, 1974.
6. Kim, H.J., Sasaki, D., Obayashi, S. and Nakahashi, K., "Aerodynamic Optimization of Supersonic Transport Wing Using Unstructured Adjoint Method," AIAA

Journal Vol.39, No.6, pp.1011-1020, 2001.

7. Vanderplaats, G.N., "ADS - A Fortran Program For Automated Design Synthesis version 3.00," Engineering Design Optimization, INC., 1987.

8. Jameson, A., "Optimum Aerodynamic Design Using CFD and Control Theory," AIAA paper 95-1729-CP, 1995.

9. Takanashi, S., "Iterative Three Dimensional Transonic Wing Design Using Integral Equations," Journal of Aircraft, Vol.22, No.8, pp.655-660, 1985.

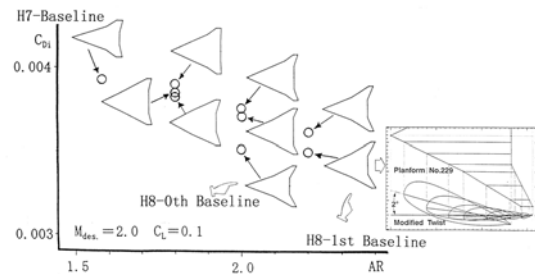
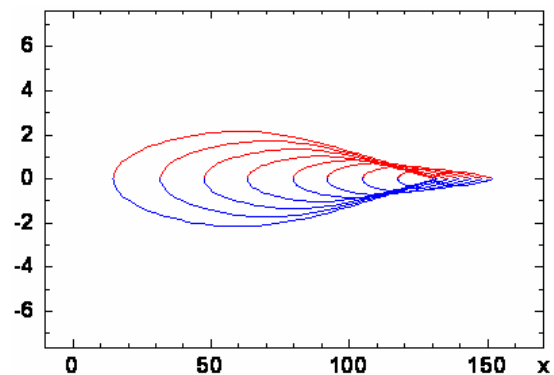
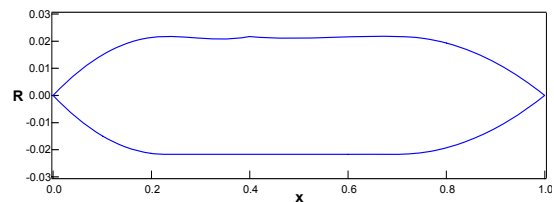


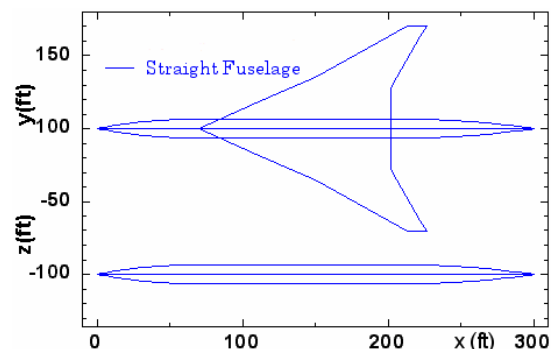
Figure 1. Wing planforms



(a) Airfoil geometries.

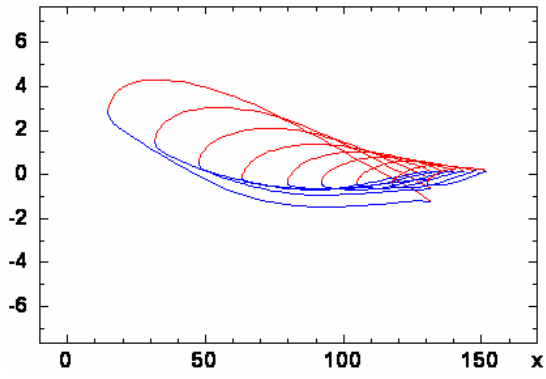


(b) Fuselage geometry

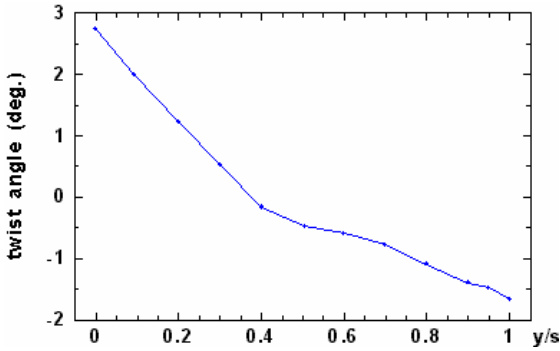


(c) Top and side view.

Figure 2. 0th configuration.



(a) Airfoil geometries.



(b) Twist angle distribution.
Figure 3. 1st configuration.

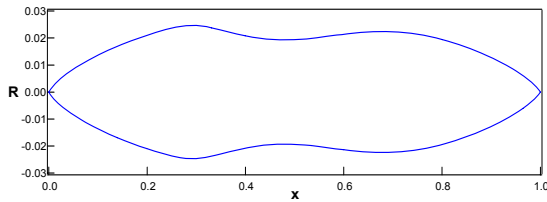
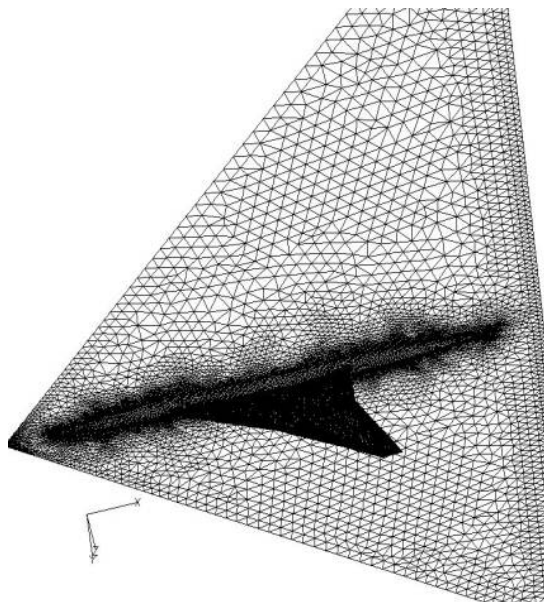
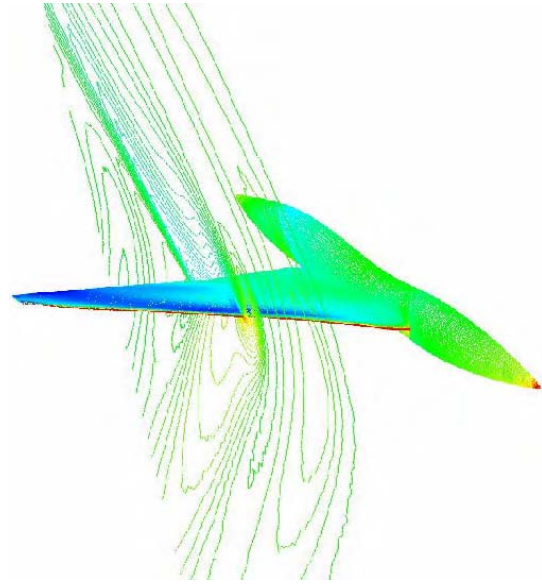


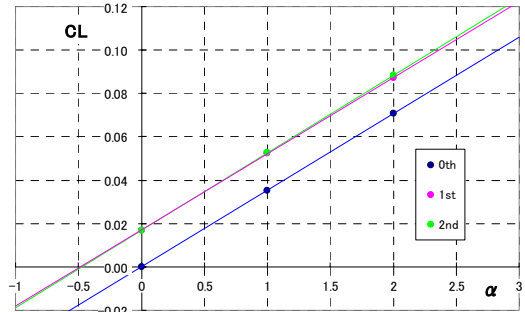
Figure 4. 2nd configuration
(area-rule fuselage).



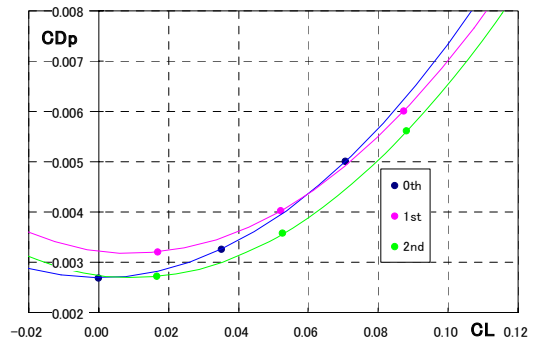
(a) Unstructured grid.



(b) Pressure contours.
Figure 5. CFD analysis.



(a) C_L - α curve.



(b) Polar curve.

Figure 6. Warp and area-rule design effect.

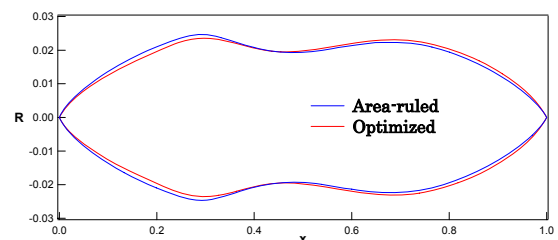
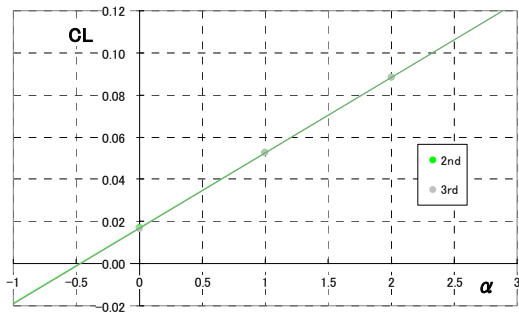
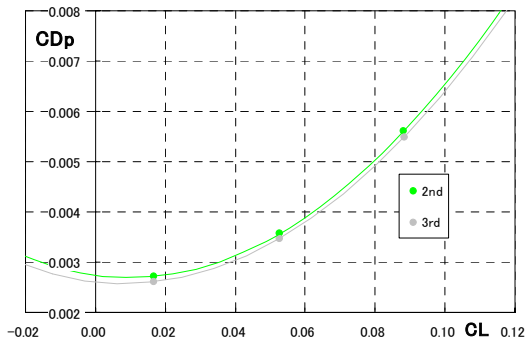


Figure 7. Optimized fuselage geometry.



(a) C_L - α curve.



(b) Polar curve.

Figure 8. Fuselage shape optimization effect.

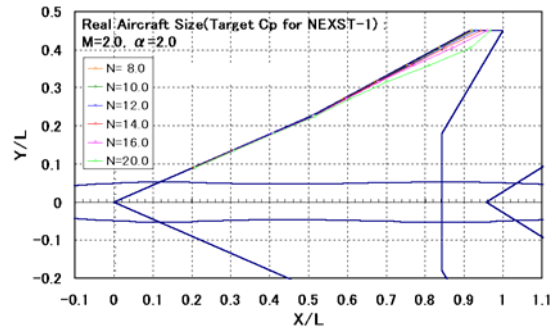


Figure 10. Transition map on target C_p at NEXST-1 flight condition.

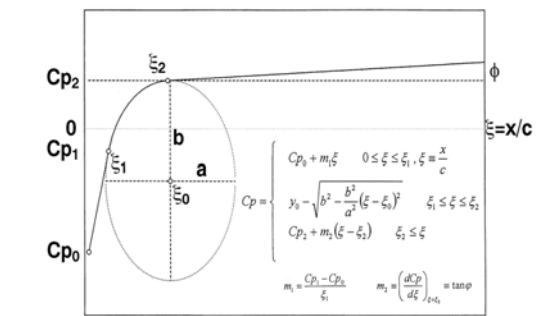


Figure 11. Parametric study on optimum target C_p .

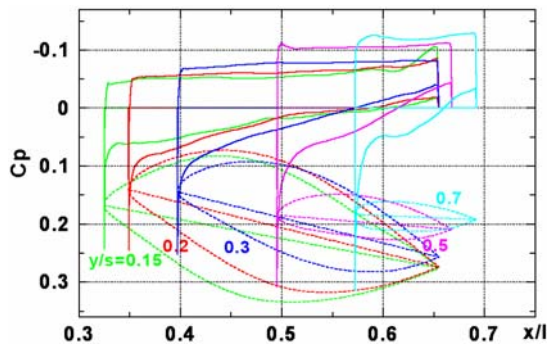


Figure 9. Target C_p for NLF wing of NEXST-1.

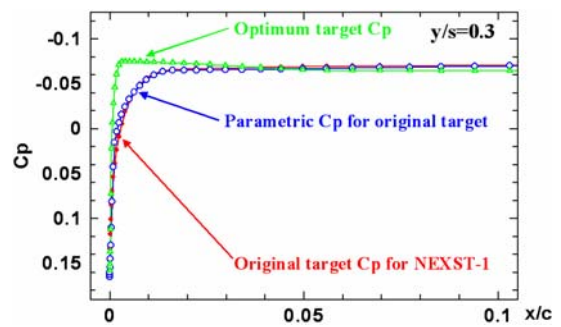


Figure 13. Optimum target C_p distribution.

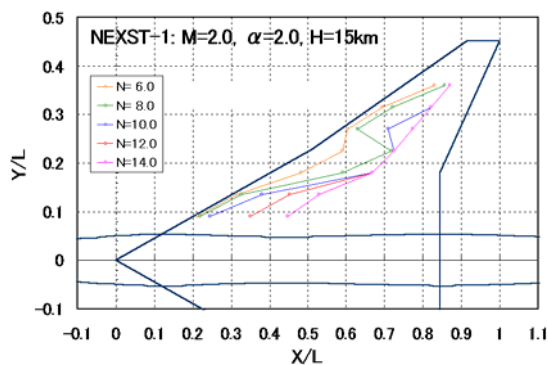


Figure 10. Transition map on target C_p at NEXST-1 flight condition.

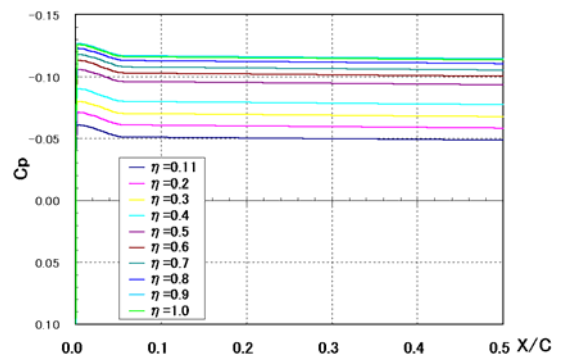


Figure 14. Target C_p distributions.

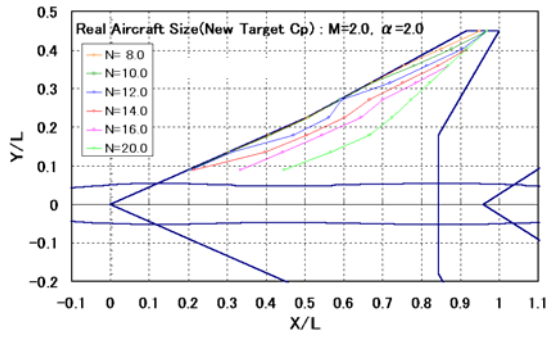


Figure 15. Transition points estimation for target Cp distributions.

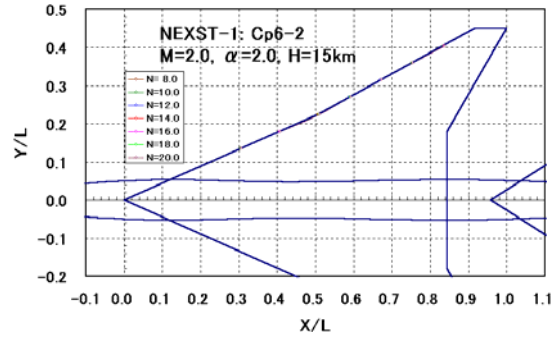


Figure 18. Transition points estimation for design Cp distributions after 7 iterations.

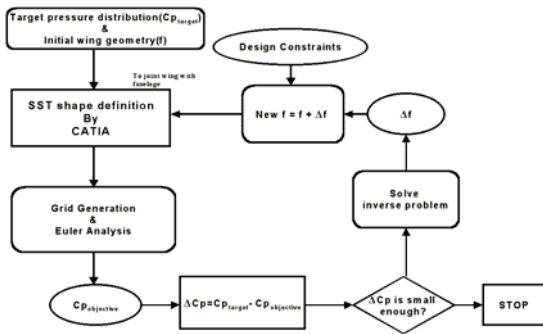
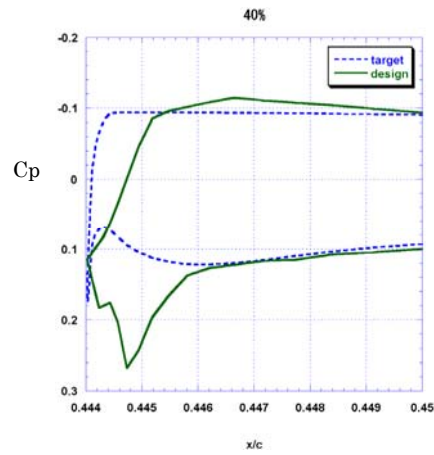
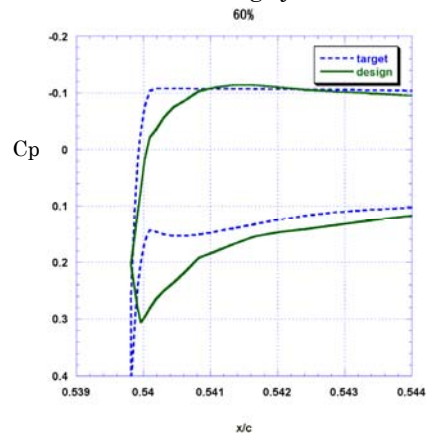


Figure 16. Flow-chart of inverse design.

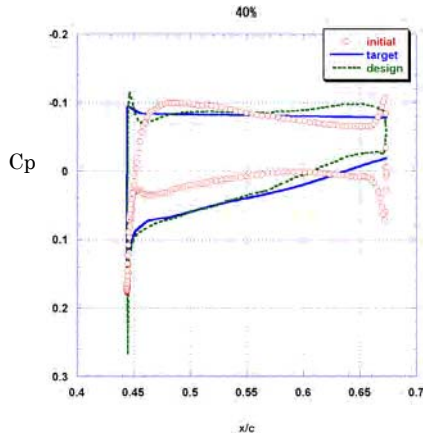


(a) inner wing (y/s=0.4).

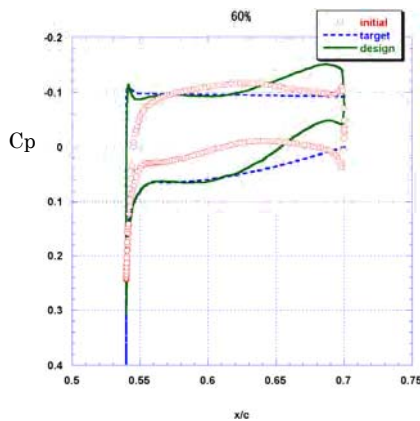


(b) outer wing (y/s=0.6).

Figure 19. Close view of Cp distributions of target and design wing after 7 iterations.



(a) inner wing (y/s=0.4).



(b) outer wing (y/s=0.6).

Figure 17. Cp distributions of initial, target and designed wing after 7 iterations.

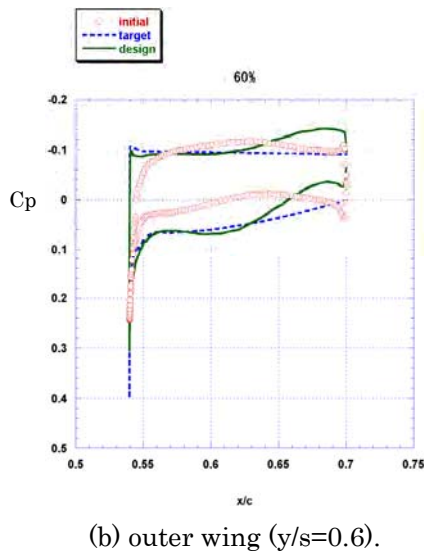
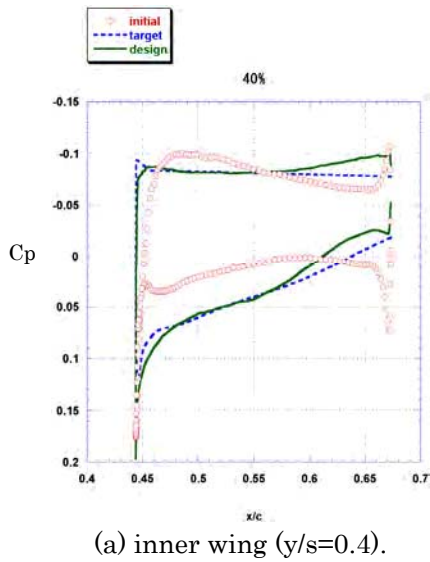


Figure 20. Cp distributions of initial, target and designed wing after 10 iterations.

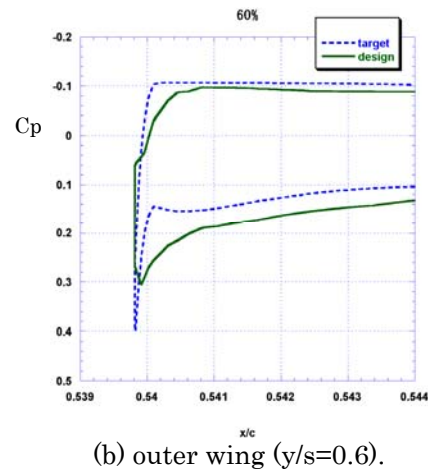
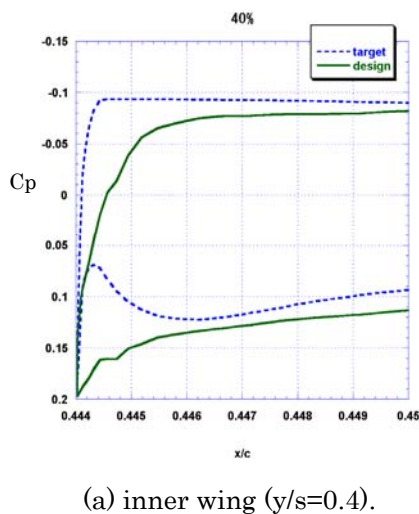


Figure 21. Close view of Cp distributions of target and design wing after 10 iterations.

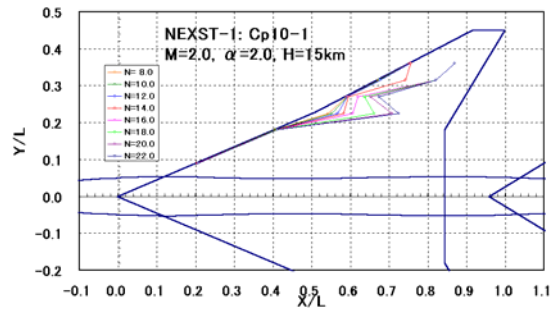


Figure 22. Transition points estimation for design Cp distributions after 10 iterations.

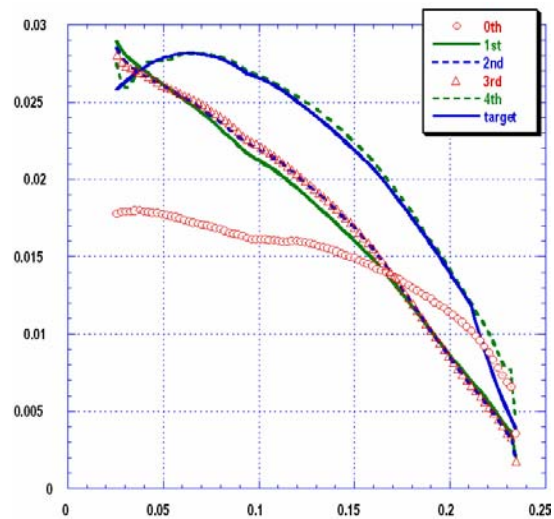
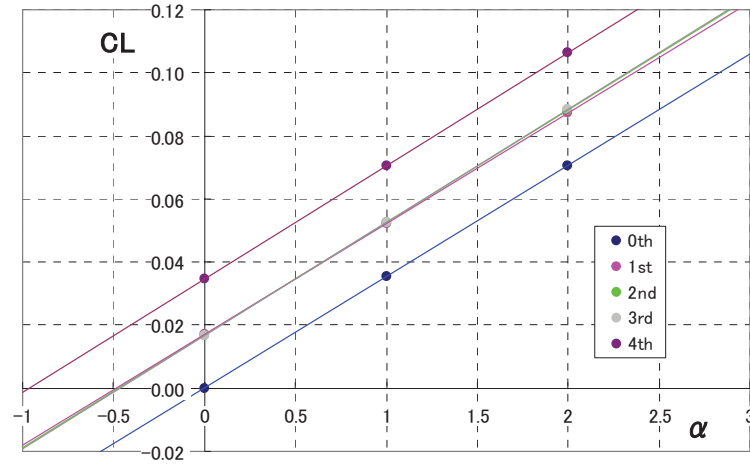
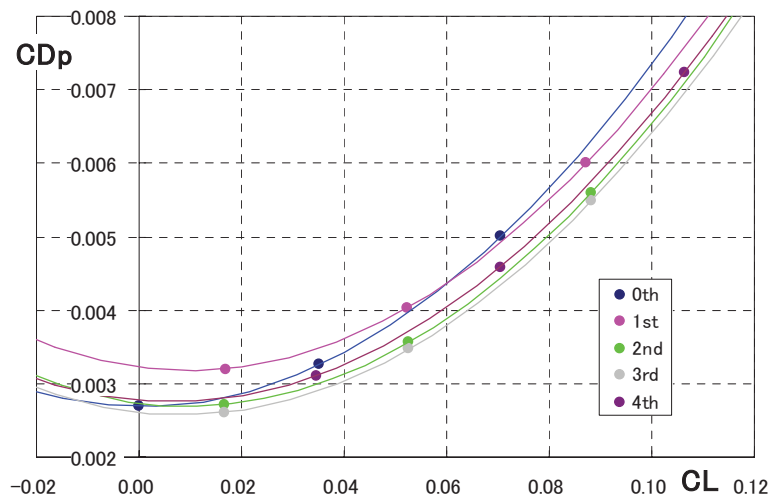


Figure 23. Spanwise load distribution.

(a) CL - α curve.

(b) Polar curve.

Figure 24. Effect of inverse design.

Table 1. Design process

Conf.	Method	Fuselage	Wing Warp	Airfoil
0 th	Empirical	Nose&Tail Cone +Straight Body	Flat	NACA 64A series
1 st	Supersonic Linear Theory	Nose&Tail Cone +Straight Body	Carlson	NACA 64A series
2 nd	Supersonic Linear Theory	Linear Area-ruled	Carlson	NACA 64A series
3 rd	Optimized by Euler	Non-linear Area-ruled	Carlson	NACA 64A series
4 th	Inverse by Euler	Non-linear Area-ruled	Carlson	Supersonic NLF Wing

Table 2. Aerodynamic properties.

Conf.	CL_α	K	CD_{p_min}	$CL@CD_{p_min}$	$CD_p@CL_{des}$	L/D_{max}	$CL@L/D_{max}$
0 th	0.035	0.470	26.9 cts	0.0004	73.5 cts	14.15	0.0756
1 st	0.035	0.470	31.8 cts	0.0097	70.1 cts	14.56	0.0828
2 nd	0.036	0.472	26.9 cts	0.0096	65.4 cts	15.94	0.0762
3 rd	0.036	0.455	25.8 cts	0.0083	64.0 cts	16.31	0.0757
4 th	0.036	0.449	27.5 cts	0.0065	66.8 cts	15.46	0.0785